Jun-Hyun Kim
Sung-Woon Cho
Chang-Koo Kim*

Angular Dependence of Si_3N_4 Etching in $C_4F_6/CH_2F_2/O_2/Ar$ Plasmas

The dependence of Si_3N_4 etching on ion-incident angles is investigated at various CH_2F_2 flow rates in $C_4F_6/CH_2F_2/O_2/Ar$ plasmas. The normalized etch yield (NEY) curves for Si_3N_4 imply that physical sputtering is a major contributor to Si_3N_4 etching. An increase in the amount of CH_2F_2 in the plasma produces thicker and more etch-resistant fluorocarbon films. Systematic analyses on deposition and etching of the passively deposited fluorocarbon films on Si_3N_4 in a $C_4F_6/CH_2F_2/O_2/Ar$ plasma show that the normalized deposition rate of the fluorocarbon film is nearly the same and unaffected by the CH_2F_2 flow rate while etching of fluorocarbon films is similar to etching of Si_3N_4, thus, etching of the fluorocarbon film, rather than its deposition, limits Si_3N_4 etching in $C_4F_6/CH_2F_2/O_2/Ar$ plasmas.

Keywords: Angular dependence, Etch yields, Fluorocarbon films, Physical sputtering, Si_3N_4 etching

Received: March 05, 2017; *revised:* October 09, 2017; *accepted:* October 11, 2017

DOI: 10.1002/ceat.201700126

1 Introduction

Silicon nitride (Si_3N_4) is a dielectric material widely applied in the fabrication of microelectronic devices. It is used primarily as insulation between conducting layers, diffusion and ion implantation masks, and passivation [1]. In recently developed ultralarge-scale integrated (ULSI) circuit technology, the role of Si_3N_4 films has grown because they serve as etch stop layers for self-aligned contact (SAC) structures and as gate spacers for the formation of doped regions [2–4]. The application of Si_3N_4 as an etch stop layer and a gate spacer requires good control over the relative etch rate of Si_3N_4, i.e., etch selectivity. For example, high silicon oxide (SiO_2)-to-Si_3N_4 etch selectivity is strongly required for SAC etching. However, the Si_3N_4 etch rate frequently increases at corners and inclined surfaces [3] resulting in low SiO_2-to-Si_3N_4 etch selectivity at curved Si_3N_4 surfaces, leading to failures in SAC etching. Therefore, it is essential to understand the angular dependence of the Si_3N_4 etch rate in order to predict and control etch selectivities and profiles.

To investigate the angular dependence of the Si_3N_4 etch rate, it is necessary to precisely control the direction of ions that are incident on the surface of a substrate. Angular dependences of Si_3N_4 etch rates using ion beam etching [5] and V-groove microstructures [6] were reported. The ion beam apparatus could control the ion-incident angle θ, but its low operating pressure depressed the radical concentration too much for plasma etching to be practical. V-groove samples enabled experiments under practical plasma etching conditions, but only a few ion-incident angles were available.

Faraday cages have been used extensively to study the angular dependences of etch rates of various surfaces [7–12]. A Faraday cage is a closed box made from a conductor. If the top plane of the cage is made from conductive grids with diameters smaller than the sheath thickness, ions will enter perpendicular to the sheath formed along it. Since the electric potential in the cage is uniform and unaffected by electric fields outside the cage, the ions travelling inside the cage maintain their initial direction. Therefore, the use of a Faraday cage allows to accurately control the direction of ions incident on the substrate under practical plasma etching conditions by simply varying the angle of the substrate inside the cage.

Lee et al. [12] reported the angular dependences of Si_3N_4 etch rates at various bias voltages in a C_4F_8 plasma using a Faraday cage. They correlated the change in the etch yield with the thickness of a steady-state fluorocarbon film formed on the substrate. They successfully observed the angular dependence of the Si_3N_4 etch rate under practical plasma etching conditions, but the discharge gas, C_4F_8, was perfluorocarbon (PFC). PFCs are problematic from an environmental viewpoint because they have long atmospheric lifetimes and high global warming potentials [13–15]. Unsaturated fluorocarbons like C_4F_6 have been considered as alternatives to PFCs [16, 17].

In this study, the angular dependences of Si_3N_4 etch rates in $C_4F_6/CH_2F_2/O_2/Ar$ plasmas were investigated using a Faraday cage system. The etching characteristics of Si_3N_4 were studied by varying the ion-incident angles and CH_2F_2 flow rates. The

Jun-Hyun Kim, Sung-Woon Cho, Prof. Chang-Koo Kim
changkoo@ajou.ac.kr
Ajou University, Department of Chemical Engineering and Department of Energy Systems Research, Worldcup-ro 206, Woncheon-dong, Yeontong-gu, Suwon 16499, Korea.

effects of CH_2F_2 were also examined by analyzing the fluorocarbon films formed on the surface of the substrate during Si_3N_4 etching.

2 Experimental

Si_3N_4 etching was performed in an inductively coupled plasma system as displayed in Fig. 1. The diameters of a reaction chamber and an electrode were 200 and 110 mm, respectively. Both the reaction chamber and electrode were made of stainless steel. The plasma was ignited in the reaction chamber by applying a 13.56-MHz radiofrequency (rf) source power to an induction coil. Another 13.56-MHz rf power was used to apply a bias power to the electrode. A quartz window was located below the induction coil, and the distance between the dielectric window and the electrode was 100 mm.

A Faraday cage was used to control the direction of ions that are incident on the sample. The Faraday cage was attached to the electrode. Fig. 2 shows a schematic diagram of the Faraday cage and the arrangement of the samples. The Faraday cage was cylindrical and made from stainless steel. The inner diameter and height of the cage were 80 and 20 mm, respectively. The top plane of the cage was a stainless-steel grid. The grid diameter and pitch were 0.025 and 0.229 mm, respectively. The ion-incident angle (θ) was defined as the angle between the ion-incident direction and the surface normal to the sample. As mentioned earlier, the sheath forms along the top plane of the cage and its interior is free of electric fields. Therefore, the angle of ions incident on a sample can be controlled by varying the angle of the sample holder. In this study, the angle of the sample holder was varied between 0 and 90°. The samples were 470 nm thick Si_3N_4 films on p-type Si wafers. The Si_3N_4 films were obtained by low-pressure chemical vapor deposition. The sample was in the form of a 10×5 mm^2 rectangle. A 1 mm thick quartz bottom plate was placed below the sample holder to mimic the hole structure of microelectronic devices.

A $C_4F_6/CH_2F_2/O_2/Ar$ plasma was used for Si_3N_4 etching. The total flow rate of the discharge gas was 40 sccm. The flow rates of C_4F_6 and O_2 were fixed at 6 and 1 sccm, respectively. The flow rate of CH_2F_2 was varied from 0 to 5 sccm. Therefore, the fraction of CH_2F_2 in the input gas, i.e., ratio of the CH_2F_2 flow rate to the total flow rate, ranged from 0 to 12.5 %. The flow rate of Ar was then modulated such that the combined flow rate of C_4F_6, CH_2F_2, O_2, and Ar was 40 sccm. The pressure in the chamber was 9 mTorr. The source power and bias voltage were 150 W and –450 V, respectively.

The etch rates of the samples were determined by measuring changes in the thickness of the substrate film before and after etching using a thickness meter (model SpecraThick 2000-Deluxe). In all cases, the thickness was measured at 8 mm from the bottom of the sample holder.

The characteristics of a fluorocarbon films formed on the Si_3N_4 surface were analyzed by X-ray photoelectron spectroscopy (XPS). The atomic ratio of fluorine to carbon in the fluorocarbon films was calculated from the C 1s XPS peaks of the film.

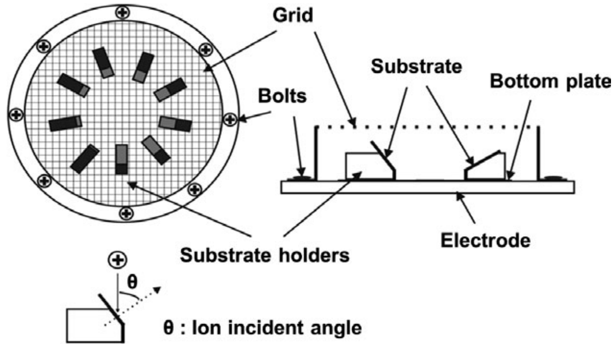

Figure 2. Schematic diagrams of a Faraday cage and the substrate arrangement in the cage. The ion-incident angle θ was defined as the angle between the ion-incident direction and the surface normal to the substrate.

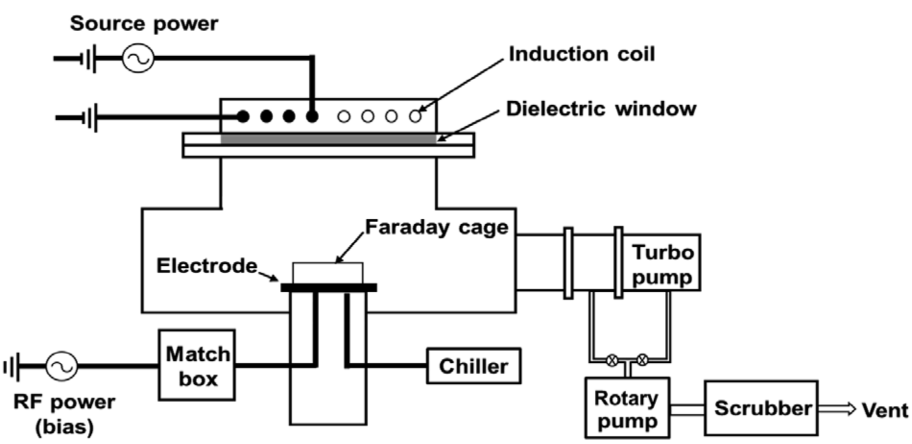

Figure 1. Schematic diagram of an inductively coupled plasma system equipped with a Faraday cage.

3 Results

Fig. 3 a shows the change in the etch rate (ER) of Si_3N_4 with the ion-incident angle at various CH_2F_2 flow rates. The etch rates decrease with increasing CH_2F_2 flow rate at all ion-incident angles. This results from the reduction in F radicals, which are etchants for Si_3N_4, by H atoms coming from CH_2F_2. H atoms can react with F radicals to form HF [17]. In the absence of CH_2F_2, the etch rate decreases monotonically with ion-incident angle. On the other hand, in the presence of CH_2F_2, the etch rates increase with ion-incident angle, reach maxima at angles about 40°, and decrease with further increase in the ion-incident angle. This behavior becomes more prominent as the fraction of CH_2F_2 in the input gas increases. This can be better observed using the nor-

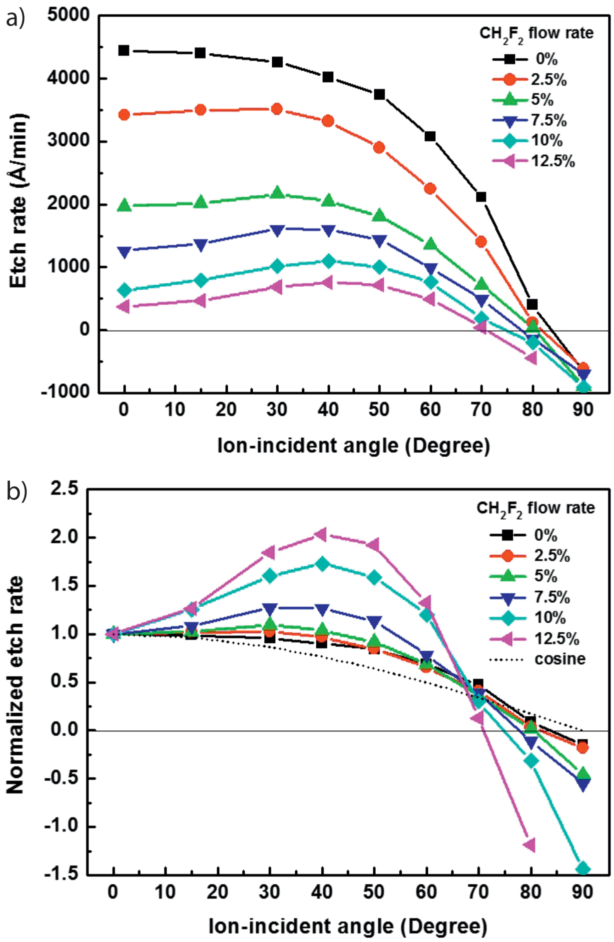

Figure 3. Angular dependences of (a) etch rates and (b) normalized etch rates of Si_3N_4 with various CH_2F_2 fractions in the input gas. The CH_2F_2 fraction was based on the total flow rate of the discharge gas.

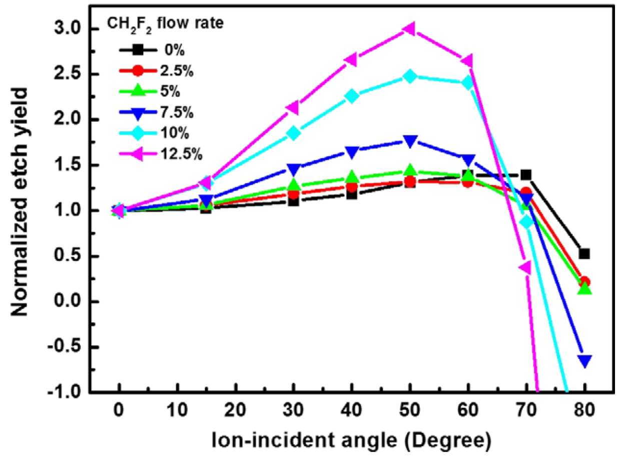

Figure 4. Angular dependences of normalized etch yields of Si_3N_4 at various CH_2F_2 flow rates.

malized etch rate (NER) curve. The NER is defined as the etch rate at a specific angle normalized to the etch rate on the horizontal surface, i.e., ER(θ)/ER(0°).

Fig. 3 b illustrates the NER of Si_3N_4 as a function of ion-incident angle with various CH_2F_2 flow rates. In the NER curve, the dotted line indicates a cosine curve representing the change in the flux of ions incident on the sample with their angles. When the CH_2F_2 fraction is increased from 0 to 12.5 %, the NERs are higher than the cosine curve at ion-incident angles between 0 to 60°. All of the NERs fall below the cosine curve when the ion-incident angle is higher than 80°. When the ion-incident angle is 90°, all the NERs are negative, indicating deposition instead of etching at this angle.

When ion-surface interactions are investigated at various ion-incident angles, it is more relevant to use the etch yield (EY) than the etch rate [7]. The etch yield is defined as the etch rate per ion flux on the substrate surface. Since ion flux is proportional to cosθ, the etch yield excludes the ion flux variations driven by the incident angle.

Fig. 4 displays the normalized etch yield (NEY) of Si_3N_4 as a function of ion-incident angle. The NEY is defined as the etch yield at a specific angle divided by the etch yield on the horizontal surface [EY(θ)/EY(0°)], which is equal to NER(θ)/cos θ. The angular dependence of the NEY exhibit maxima between 50 and 70° at all CH_2F_2 flow rates. In the absence of CH_2F_2, the NEY exhibits maxima at 70°. As the CH_2F_2 fraction in the input gas is increased to 12.5 %, the maximum NEY increases to 3.0 and the angle at which the maximum is reached declines from 70 to 50°.

The shapes of the etch yield curves provide information on the etching mechanism. Possible mechanisms include ion-enhanced chemical etching and physical sputtering [18]. When ion-enhanced chemical etching dominates, the etch yield decreases monotonically with the ion-incident angle. On the other hand, when physical sputtering dominates, the etch yield exhibits maxima at angles between 40 and 70°. The NEY curves of Si_3N_4 in Fig. 4 suggest that physical sputtering is a major contributor to Si_3N_4 etching in $C_4F_6/CH_2F_2/O_2/Ar$ plasmas. However, the maximum NEY value and the ion-incident angle at which this maximum is observed change with the CH_2F_2 flow rate. This means that the extent to which physical sputtering contributes to Si_3N_4 etching is dependent on the amount of CH_2F_2 used.

4 Discussion

When a substrate is exposed to fluorocarbon plasmas, e.g., C_4F_6, fluorocarbon polymer (-C_xF_y-) films grow on the surface of the substrate. At the same time, the fluorocarbon films are consumed by ion sputtering, F-atom etching, and ion-assisted interactions between the fluorocarbon film and the substrate [4]. At the steady state, a thin fluorocarbon film forms on the substrate surface as a result of competition between fluorocarbon production and consumption. Then, Si_3N_4 substrate etching occurs by forming volatile species such as SiF_x and CNF_y via ion bombardment, F-atom interactions, and fluorocarbon film-Si_3N_4 interactions. The fluorocarbon film formed on the substrate during etching in fluorocarbon plasmas plays an important role because it acts as an etch barrier against radicals and ions [7]. As indicated in Fig. 4, the angular dependence of the NEY depended on the CH_2F_2 flow rate. Therefore, the characteristics of the fluorocarbon film must be investigated.

Fig. 5 a displays changes in the deposition rates of passively deposited fluorocarbon films on Si_3N_4 with the ion-incident angle at various CH_2F_2 flow rates. During fluorocarbon film deposition, no bias voltage was applied to the substrate. Except for the bias voltage, the other process conditions were the same as those used in Si_3N_4 etching: 150 W source power, 9 mTorr pressure, 40 sccm total flow rate of $C_4F_6/CH_2F_2/O_2/Ar$. The deposition rates of the fluorocarbon films increase with CH_2F_2 flow rate at all ion-incident angles. This is because the addition of CH_2F_2 provides reactive fluorocarbon species such as CF_2. Since CF_2 radicals are known to be the main precursors for fluorocarbon film formation in fluorocarbon plasmas [16], thicker fluorocarbon films are deposited on the substrate as more CH_2F_2 is introduced.

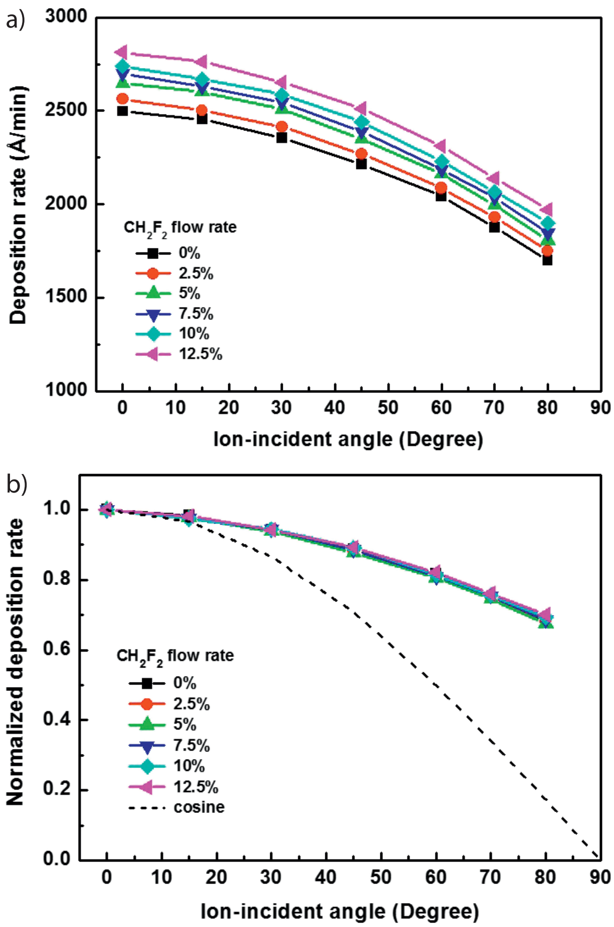

Figure 5. Angular dependences of (a) deposition rates and (b) normalized deposition rates of passively deposited fluorocarbon films on Si_3N_4 in a $C_4F_6/CH_2F_2/O_2/Ar$ plasma at various CH_2F_2 flow rates.

The deposition rates of the fluorocarbon films decrease monotonically with increasing ion-incident angle at all CH_2F_2 flow rates. In order to clarify the angular dependence of the change in the deposition rate with the CH_2F_2 flow rate, the normalized deposition rate (NDR) was plotted at various CH_2F_2 flow rates in Fig. 5 b. Similarly to the definition of the normalized etch rate (see Fig. 3 b), the NDR is defined as the deposition rate (DR) at a specific angle normalized to the deposition rate on the horizontal surface, i.e., $DR(\theta)/DR(0°)$. The NDR presented in Fig. 5 b nearly falls on a single curve, regardless of the CH_2F_2 flow rate. This implies that Si_3N_4 etching is not limited by deposition of the fluorocarbon film although its deposition rate increases with the CH_2F_2 flow rate.

Fig. 6 shows fluorine-to-carbon (F/C) ratios of passively deposited fluorocarbon films deposited at various fractions of CH_2F_2. The F/C ratios were obtained from the carbon 1s X-ray photoemission spectra of the films [4]. For analysis of the F/C ratio, the fluorocarbon films deposited at an ion-incident angle of 0° were used. The F/C ratio of the fluorocarbon film decreases with increasing CH_2F_2 flow rate. As mentioned earlier, H atoms from CH_2F_2 can react with F to form HF. This reduces the number of F radicals in the plasma, and produces a more fluorine-depleted fluorocarbon film. These defluorinated fluorocarbon films have high etch resistance because of an increase in the carbon-to-carbon cross-linking of the film [17].

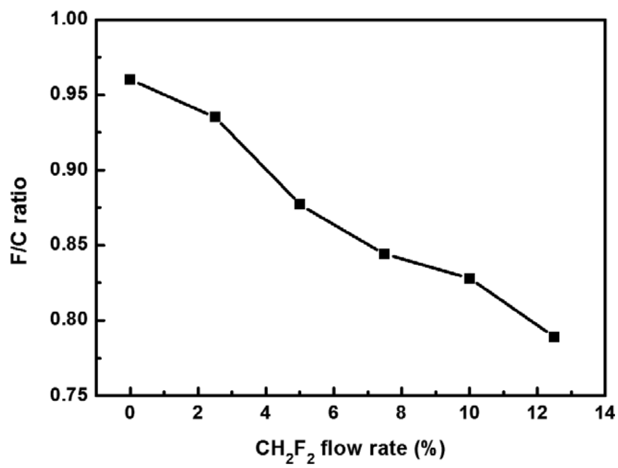

Figure 6. F/C ratios of passively deposited fluorocarbon films deposited at various CH_2F_2 flow rates. The ion-incident angle was 0°.

This relationship between etch resistance of the fluorocarbon film and CH_2F_2 flow rate was confirmed by etching the fluorocarbon film. Fig. 7 presents the etch rates and NERs of passively deposited fluorocarbon films on Si_3N_4 in $C_4F_6/CH_2F_2/O_2/Ar$ plasmas as a function of the ion-incident angle at various CH_2F_2 flow rates. The fluorocarbon films were etched under the same conditions as those for Si_3N_4 etching. As expected, the etch rate of the fluorocarbon film decreases with increasing CH_2F_2 flow rate at all ion-incident angles. It is interesting to note that the shapes of the etch rate, or even NER, versus ion-incident angle curves from fluorocarbon film etching are very similar to those produced during Si_3N_4 etching (see Fig. 3). When CH_2F_2 is absent (0 %), the etch rate of the fluorocarbon film decreases monotonically with the ion-incident angle. However, when CH_2F_2 is added, the etch rate of the film rises, reaches a maximum at 50°, and declines with increasing ion-incident angle.

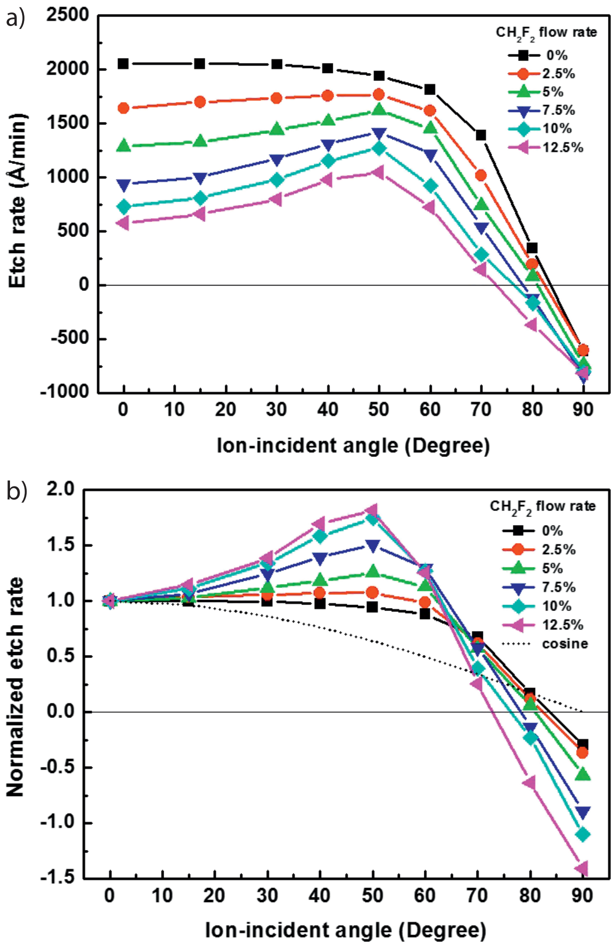

Figure 7. Angular dependences of (a) etch rates and (b) normalized etch rates of passively deposited fluorocarbon films on Si_3N_4 in a $C_4F_6/CH_2F_2/O_2/Ar$ plasma at various CH_2F_2 flow rates.

The similarities between the angular dependences of the etch rates of the fluorocarbon film and Si_3N_4 substrate can be more clearly seen by analyzing the normalized etch yield (NEY). Fig. 8 illustrates the NEYs of the passively deposited fluorocarbon films on Si_3N_4 as a function of the ion-incident angle with various CH_2F_2 flow rates. Much like the NEY curve from Si_3N_4 etching (see Fig. 4), the NEY in this experiment exhibits a maximum at 70° in the absence of CH_2F_2. Furthermore, as the CH_2F_2 fraction increases to 12.5 %, the maximum NEY increases and the angle at which it is reached changes from 70 to 50°.

As indicated in the graph that relates the NDR of the fluorocarbon film and the ion-incident angle at various CH_2F_2 flow rates (Fig. 5 b), the deposition of fluorocarbon films dose not play an important role in determining Si_3N_4 etch characteristics in $C_4F_6/CH_2F_2/O_2/Ar$ plasmas. On the other hand, there are similarities between etching of fluorocarbon films and Si_3N_4. Therefore, fluorocarbon film etching, rather than deposition, limits etching of Si_3N_4 in $C_4F_6/CH_2F_2/O_2/Ar$ plasmas.

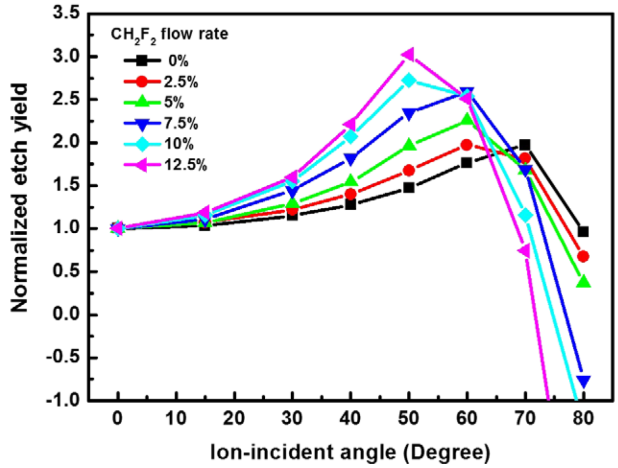

Figure 8. Angular dependences of normalized etch yields of passively deposited fluorocarbon films on Si_3N_4 in a $C_4F_6/CH_2F_2/O_2/Ar$ plasma at various CH_2F_2 flow rates.

5 Conclusions

The angular dependence of Si_3N_4 etching in $C_4F_6/CH_2F_2/O_2/Ar$ plasmas was investigated at various CH_2F_2 flow rates. The etch rates of Si_3N_4 decreased monotonically with the ion-incident angle in the absence of CH_2F_2 while they exhibited maxima at angles around 40° in the presence of CH_2F_2. The normalized etch yield (NEY) curves of Si_3N_4 showed maxima at angles between 50 and 70° at all CH_2F_2 flow rates, indicating that physical sputtering was a major contributor to Si_3N_4 etching in $C_4F_6/CH_2F_2/O_2/Ar$ plasmas. In addition, the maximum NEY and the ion-incident angle at which it was reached were affected by the CH_2F_2 flow rate.

The deposition rates of the passively deposited fluorocarbon films on the substrate increased with CH_2F_2 flow rate at all ion-incident angles because the addition of CH_2F_2 provided more CF_2, which is the main precursor for the formation of fluorocarbon films. Although the deposition rate of the fluorocarbon film changed with the CH_2F_2 flow rate, its normalized deposition rate (NDR) fell on a single curve, regardless of the CH_2F_2 flow rate.

The variations in the CH_2F_2 flow rate also affected the etch rate of the passively deposited fluorocarbon film via its F/C ratio. The F/C ratio of the fluorocarbon film decreased and the film became more defluorinated with increasing CH_2F_2 flow rate. This was driven by F reduction by H atoms from CH_2F_2. Due to an increase in the etch resistance of the defluorinated fluorocarbon film, the etch rate of the fluorocarbon film declined with rising CH_2F_2 flow rate at all ion-incident angles.

There were close similarities between etching of fluorocarbon films and Si_3N_4. The NEYs of both materials exhibited maxima at 70°. As the CH_2F_2 flow rate was increased to 12.5 %, the maximum NEY became higher and the angle at which it was achieved changed to 50°. Thus, fluorocarbon film etching, rather than deposition, is a limiting factor for Si_3N_4 etching in $C_4F_6/CH_2F_2/O_2/Ar$ plasmas.

Acknowledgment

This work was supported by the National Research Foundation of Korea (NRF) grant funded by the Korea government (MEST) (Grant No. 2015R1A2A2A01002305) and the GRRC program of Gyeonggi province (GRRC AJOU 2017B03, Photonics-Medical Convergence Technology Research Center).

The authors have declared no conflict of interest.

Abbreviations

DR	deposition rate
ER	etch rate
EY	etch yield
NDR	normalized deposition rate
NER	normalized etch rate
NEY	normalized etch yield
PFC	perfluorocarbon
rf	radiofrequency
SAC	self-aligned contact
ULSI	ultralarge-scale integrated
XPS	X-ray photoelectron spectroscopy

References

[1] Y. X. Li, P. J. French, R. F. Wolffenbuttel, *J. Vac. Sci. Technol., B: Microelectron. Nanometer Struct. – Process., Meas., Phenom.* **1995**, *13 (5)*, 2008–2012. DOI: 10.1116/1.588124

[2] M. Ito, K. Kamiya, M. Hori, T. Goto, *J. Appl. Phys.* **2002**, *91 (5)*, 3452–3458. DOI: 10.1063/1.1448870

[3] M. Schaepkens, G. S. Oehrlein, C. Hedlund, L. B. Jonsson, H.-O. Blom, *J. Vac. Sci. Technol., A* **1998**, *16 (6)*, 3281–3286. DOI: 10.1116/1.581534

[4] M. Schaepkens, T. E. F. M. Standaert, N. R. Rueger, P. G. M. Sebel, G. S. Oehrlein, J. M. Cook, *J. Vac. Sci. Technol., A* **1999**, *17 (1)*, 26–37. DOI: 10.1116/1.582108

[5] A. M. Barklund, H.-O. Blom, *J. Vac. Sci. Technol., A* **1992**, *10 (4)*, 1212–1216. DOI: 10.1116/1.578229

[6] A. M. Barklund, H.-O. Blom, *J. Vac. Sci. Technol., A* **1993**, *11 (4)*, 1226–1229. DOI: 10.1116/1.578497

[7] B.-O. Cho, S.-W. Hwang, G.-R. Lee, S. H. Moon, *J. Vac. Sci. Technol., A* **2000**, *18 (6)*, 2791–2798. DOI: 10.1116/1.1318193

[8] J.-H. Min, G.-R. Lee, J.-K. Lee, S. H. Moon, C.-K. Kim, *J. Vac. Sci. Technol., A* **2004**, *22 (3)*, 661–669. DOI: 10.1116/1.1722680

[9] J.-H. Min, G.-R. Lee, J.-K. Lee, C.-K. Kim, S. H. Moon, *Surf. Coat. Technol.* **2005**, *23 (1–3)*, 75–80. DOI: 10.1016/j.surfcoat.2004.08.153

[10] S.-W. Hwang, G.-R. Lee, J.-H. Min, S. H. Moon, *Surf. Coat. Technol.* **2003**, *174–175 (1)*, 835–838. DOI: 10.1016/S0257-8972(03)00561-9

[11] S.-W. Hwang, G.-R. Lee, J.-H. Min, S. H. Moon, *Electrochem. Solid-State Lett.* **2003**, *6 (1)*, G12–G15. DOI: 10.1149/1.1524750

[12] J.-K. Lee, G.-R. Lee, J.-H. Min, S. H. Moon, *J. Vac. Sci. Technol., A* **2007**, *25 (5)*, 1395–1401. DOI: 10.1116/1.2757180

[13] L. Pruette, S. Karecki, R. Reif, L. Tousignant, W. Reagan, S. Kesari, L. Zazzera, *J. Electrochem. Soc.* **2000**, *147 (3)*, 1149–1153. DOI: 10.1149/1.1393328

[14] S. Karecki, R. Chatterjee, L. Pruette, R. Reif, T. Sparks, L. Beu, V. Vartanian, K. Novoselov, *J. Electrochem. Soc.* **2001**, *148 (3)*, G141–G149. DOI: 10.1149/1.1348263

[15] R. Chatterjee, S. Karecki, R. Reif, V. Vartanian, T. Sparks, *J. Electrochem. Soc.* **2002**, *149 (4)*, G276–G285. DOI: 10.1149/1.1457988

[16] H.-K. Ryu, B.-S. Lee, S.-K. Park, I.-W. Kim, C.-K. Kim, *Electrochem. Solid-State Lett.* **2003**, *6 (9)*, C126–C129. DOI: 10.1149/1.1594412

[17] S.-W. Cho, C.-K. Kim, J.-K. Lee, S. H. Moon, H. Chae, *J. Vac. Sci. Technol., A* **2012**, *30 (5)*, 051301. DOI: 10.1116/1.4732127

[18] D. P. Hamblen, A. Cha-Lin, *J. Electrochem. Soc.* **1988**, *135 (7)*, 1816–1822. DOI: 10.1149/1.2096138

